Diffuse interface model of multicomponent vesicle adhesion and fusion

Yanxiang Zhao*
Department of Mathematics, The Pennsylvania State University, University Park, Pennsylvania 16802, USA

Qiang Du†
Department of Mathematics and Department of Materials Science and Engineering, The Pennsylvania State University, University Park, Pennsylvania 16802, USA

(Received 23 October 2010; revised manuscript received 13 May 2011; published 7 July 2011)

Prefusion and postfusion states of the biological fusion process between lipid bilayer vesicle membranes are studied in this paper. Based on the Helfrich-type continuum theory, a diffuse interface model is developed which describes the phase changes on the deformable vesicles via a scalar phase field function, and incorporates the adhesion effect between the different phases of the vesicles through a nonlocal interaction potential. Various equilibrium configurations in the prefusion and postfusion states are examined. The effects of spontaneous curvatures, bending, and Gaussian rigidities on the fusion process are discussed. Instead of considering only the regions in close contact as in many previous studies, the present approach allows us to include the energetic contributions from all parts of the vesicles. By carrying out simulations based on the gradient flow of the associated energy functional, we are also able to elucidate the dynamic transitions between the prefusion and postfusion states.

DOI: 10.1103/PhysRevE.84.011903 PACS number(s): 87.16.D−, 82.70.Uv, 87.17.Rt

I. INTRODUCTION

The lipid bilayer membrane fusion process is an important cellular mechanism, which plays a critical role in many biological processes such as exocytosis, endocytosis, and pathogen entry into host cells [1–3]. It is generally viewed as comprised of three fundamental states: prefusion, hemifusion, and postfusion [3,4].

There have been many works devoted to the study of the cellular mechanisms which may induce the fusion process. For instance, the hemifusion structures, which represent intermediate states of the fusion process, have been confirmed by electrophysiological measurements [5,6]. The conditions leading to a fusion process have been examined in [7–9]. Additionally, theoretical studies have aimed at modeling fusion processes and detecting the key factors contributing to the membrane fusion. In particular, a popular continuum approach based on the elasticity of lipid bilayer membranes has been given by the stalk model [10–14], which focuses on energetic comparisons between postfusion and prefusion states and determines the conditions under which the postfusion state is energetically more favorable than the prefusion state and, consequently, membranes tend to fuse. There have also been various computational approaches, like Monte Carlo simulations [15], Brownian dynamics simulations [16,17], and dissipative particle dynamics [18,19], which have been applied to model the fusion process as well.

In this study, our starting point is the Helfrich-type bending elasticity model for multicomponent vesicles. We take surface area and volume conservations into consideration. Motivated by recent works [20,21], we also incorporate the adhesion effect and the contributions of Gaussian curvature into the continuum model. As our first attempt, we mainly consider the two equilibrium states before and after the fusion process, namely, the prefusion state where two closely apposed vesicles undergo adhesive interactions which results in the shape deformations, and the postfusion state where the merger of vesicles results in a larger two-component vesicle.

We note that our approach, which is different from the stalk models that mainly are confined to the localized close-contact region of the two apposed vesicles, allows us to study the energetic contributions from a number of possible sources and from all parts of the vesicles. Many of the factors under consideration here have not been incorporated by the stalk model, but are important to the fusion process. For example, it has been suggested that adhesion might play an important role in facilitating the membrane fusion process [1,22]. As two apposed vesicle membranes get close, they may adhere and eventually fuse into a larger one. Such an adhesion-induced fusion process has been observed for vesicles attracted by a gold surface and for lecithin membranes at the air-water interface [22]. The roles played by the adhesion on the membrane fusion process should thus be more closely studied. Similarly, due to the topological change from prefusion to postfusion, the energetic contribution of the Gaussian curvature could also be an important factor enhancing the vesicle fusion, as suggested in [20,22].

Based on a diffuse interface formulation of our continuum model, we demonstrate that various possible equilibrium configurations associated with the multicomponent vesicle fusion process, in particular the prefusion and postfusion states, can be constructed. The interplay of adhesion potential, bending, and Gaussian rigidities on the vesicle fusion can be examined through the energy comparisons of the equilibrium configurations. The contrast of bending rigidities of the separated vesicles can also be considered as the fusion process could involve vesicles with possibly different compositions.

*zhao@math.psu.edu
†qdu@math.psu.edu

 ©2011 American Physical Society

II. ENERGY CONTRIBUTIONS TO THE PREFUSION AND POSTFUSION STATES

In this section, we describe the modeling of the prefusion and postfusion states, and then focus on the axisymmetric case.

A. Prefusion

Prefusion is a state where two apposed vesicle membranes are in close contact with each other due to the adhesive interaction. Let us denote the two vesicle membranes in the prefused state by two surfaces, Γ_1 and Γ_2. The equilibrium shapes of the two prefused vesicles are determined by minimizing a total energy comprising the elastic bending energy of the vesicles and the adhesion energy between them. The elastic bending energies of Γ_i, $i = 1,2$, introduced by Helfrich [23], are of the form

$$E_{\mathrm{b},i}^{\mathrm{pre}} = \int_{\Gamma_i} \left[\kappa_H^i (H - a^i)^2 + \kappa_G^i K\right] \mathrm{d}\mathbf{x}, \quad i = 1,2, \tag{1}$$

where $H = (k_1 + k_2)/2$ and $K = k_1 k_2$ are the mean and Gaussian curvatures of Γ_i, with k_1, k_2 being the two principal curvatures. $\{\kappa_H^i\}_{i=1}^2$ and $\{\kappa_G^i\}_{i=1}^2$ are the mean curvature bending moduli and the Gaussian curvature bending moduli, respectively, and $\{a^i\}_{i=1}^2$ are the spontaneous curvatures. The adhesion energy between the two vesicles is given by the following double integral:

$$E_{\mathrm{a}}^{\mathrm{pre}} = \int_{\Gamma_1}\int_{\Gamma_2} W(|\mathbf{x}_1 - \mathbf{x}_2|)\mathrm{d}\mathbf{x}_2\mathrm{d}\mathbf{x}_1, \tag{2}$$

where the scalar-valued function W presents the adhesion potential, which is taken as a function of the distance $|\mathbf{x}_1 - \mathbf{x}_2|$ between the two points $\{\mathbf{x}_i \in \Gamma_i\}_{i=1}^2$ on different vesicles. One typical choice for W, which is adopted in this paper, is of the Leonard-Jones form

$$W(|\mathbf{x}_1 - \mathbf{x}_2|) = -4w\left[\left(\frac{\beta}{|\mathbf{x}_1 - \mathbf{x}_2|}\right)^{\alpha} - \left(\frac{\beta}{|\mathbf{x}_1 - \mathbf{x}_2|}\right)^{\alpha/2}\right], \tag{3}$$

where w measures the strength of the adhesive interaction between Γ_1 and Γ_2. The constant β and the exponent α determine the thickness of the repulsive region and the rate of change of the adhesion potential, respectively.

Combining all of the contributions to the total energy together, the equilibrium shapes of the two interactive vesicle membranes in the prefusion state is given by the minimum of

$$E^{\mathrm{pre}} = E_{\mathrm{b},1}^{\mathrm{pre}} + E_{\mathrm{b},2}^{\mathrm{pre}} - E_{\mathrm{a}}^{\mathrm{pre}}. \tag{4}$$

The enclosed volume and total area of each individual vesicle membrane are assumed to be constants. Thus the following constraints must hold:

$$\int_{\Gamma_i} \mathrm{d}\mathbf{x} = \mathrm{A}_i, \quad \int_{\Omega_i} \mathrm{d}V = \mathrm{V}_i, \quad i = 1,2, \tag{5}$$

where $\{\Omega_i\}_{i=1}^2$ represent the interior enclosed domains by $\{\Gamma_i\}_{i=1}^2$.

B. Postfusion: A diffuse interface formulation

Postfusion is the state where two prefused vesicle membranes, Γ_1 and Γ_2, merge together and fuse into a two-component vesicle Γ of a larger size. Symbolically, one has

$$\Gamma = \Gamma_1 \cup \Gamma_2,$$

with the individual surface areas being preserved and the total volume being the sum of two individual volumes from prefusion.

To simplify our discussion, we assume that the Gaussian bending moduli $\kappa_G^1 = \kappa_G^2$, both of which are equal to the Gaussian bending moduli κ_G of the fused vesicle. By the Gauss-Bonnet formula, in the prefused state, the Gaussian curvature term makes a contribution that is constantly equal to $2\pi\kappa_G\chi_{\mathrm{pre}}$, while in the fused state, the Gaussian energy is constantly equal to $2\pi\kappa_G\chi_{\mathrm{post}}$. Here χ represents the Euler number, which is uniquely determined by the topology of the membrane shape.

Since the postfusion state presents a two-component vesicle membrane with potentially different bending moduli and spontaneous curvatures on different components, it is effective to describe the membrane surface with a phase field labeling function $\eta = \eta(\mathbf{x})$ and reformulate the energy using a diffuse interface description.

More precisely, a phase field function η is introduced over the fused membrane Γ to distinguish the two components, Γ_1 and Γ_2. In the Γ_1 phase, η is specified to be nearly $+1$ (solid blue curves in Fig. 1); in the Γ_2 phase, η is assigned to be nearly -1 (dashed red curves in Fig. 1). In the interfacial region between the two phases, η makes a rapid but smooth transition. The total energy in terms of the phase field function η is given by

$$\begin{aligned} E^{\mathrm{post}}(\eta) = &\int_{\Gamma} \kappa_H(\eta)[H - a(\eta)]^2 \mathrm{d}\mathbf{x} + 2\pi\kappa_G\chi_{\Gamma} \\ &+ \sigma\int_{\Gamma}\left[\frac{\xi}{2}|\nabla_{\Gamma}\eta|^2 + \Phi(\eta)\right]\mathrm{d}\mathbf{x} \\ &- \int_{\Gamma}\int_{\Gamma} W(|\mathbf{x}_1 - \mathbf{x}_2|)G(\mathbf{x}_1,\mathbf{x}_2)\mathrm{d}\mathbf{x}_1\mathrm{d}\mathbf{x}_2, \end{aligned} \tag{6}$$

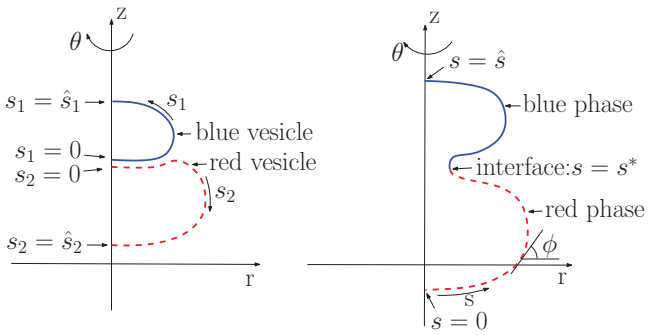

FIG. 1. (Color online) Schematic diagrams of axisymmetric case for the prefusion and postfusion states. The left graph shows a prefusion state with blue and red color indicating the vesicles with higher and lower bending moduli. The right graph shows a postfusion state with blue and red color indicating the different phases originating from vesicles in a prefusion state. The curves are parameterized by arc length, where $s = s^*$ specifies the phase boundary. ϕ is the angle of inclination from the horizontal axis, and θ is the angle of rotation.

where $\kappa_H(\eta)$ can be viewed as an inhomogeneous bending moduli, $a(\eta)$ is an inhomogeneous spontaneous curvature, and ξ controls the interfacial width. In this paper, we simply take κ_H and a to be linear functions of η:

$$\kappa_H(\eta) = \kappa_0(1 + c_H\eta), \quad a(\eta) = a_0(1 + a_H\eta). \tag{7}$$

The first term in (6) is effectively the diffuse interface description for elastic bending energy. When $\mathbf{x}$ is away from the interfacial region, η approximately takes the value of ± 1, and

$$\kappa_H(+1) \approx \kappa_H^1, \quad \kappa_H(-1) = \kappa_H^2; \quad a(+1) \approx a^1, \quad a(-1) \approx a^2.$$

The third term in (6) is a diffuse interface approximation of line tension energy, where a double well potential function

$$\Phi(\eta) = \frac{1}{4\xi}(\eta^2 - 1)^2 \tag{8}$$

is incorporated. The function $G(\mathbf{x}_1,\mathbf{x}_2)$ in the last term is of the form

$$G(\mathbf{x}_1,\mathbf{x}_2) = \frac{1}{2}\left|\frac{\eta(\mathbf{x}_1) - \eta(\mathbf{x}_2)}{2}\right|^2, \tag{9}$$

which implies that, only when $\mathbf{x}_1,\mathbf{x}_2$ are in different phases, the function $G(\mathbf{x}_1,\mathbf{x}_2)$ takes a nonzero value. In other words, the adhesive interaction only occurs between the two different phases. To avoid treating the singularity at $\mathbf{x}_1 = \mathbf{x}_2$, we replace the term $|\mathbf{x}_1 - \mathbf{x}_2|$ of (6) by $\sqrt{|\mathbf{x}_1 - \mathbf{x}_2|^2 + \epsilon}$ in the actual numerical experiments, with ϵ being a sufficiently small positive regularization constant (which is taken as 0.02 in the numerical results reported in the next section). The surface area and volume constraints are given by

$$\int_\Gamma d\mathbf{x} = A_1 + A_2, \quad \int_\Gamma \eta(\mathbf{x})d\mathbf{x} = A_1 - A_2, \quad \int_\Omega dV = V_1 + V_2, \tag{10}$$

where Ω is the entire enclosed interior domain of Γ.

Similarly as in [21], a matched asymptotic expansion can be carried out to show that the phase field function η approaches to a hyperbolic tangent (tanh) profile of the distance function as the interfacial width ξ goes to zero. Consequently, the last integral of (6) and the integral (2) differ by only an $o(\xi)$ term. Additionally, as ξ approaches 0, the first two constraints in (10) imply area conservation in (5). All of these analyses substantiate the convergence of the diffuse interface formulation to the sharp interface description of two-component vesicle membranes. For more works related to the diffuse interface models for two-component vesicles, we refer to [24–34] and the additional references given in [35]. The newly introduced adhesion terms do not lead to any extra difficulty in the asymptotic analysis, but do present additional complications in the numerical simulation of full three-dimensional (3D) vesicles. We thus study the axisymmetric setting first.

C. The axisymmetric setting

In the following, we consider the axisymmetric case where our model can be further simplified to facilitate numerical calculations. Figure 1 schematically presents the prefusion and postfusion states of two vesicles, labeled by solid blue and dashed red curves.

In the prefusion state, the two vesicle membranes are represented by rotating two curves,

$$l_1 = [r_1(s_1), z_1(s_1)], \quad l_2 = [r_2(s_2), z_2(s_2)], \tag{11}$$

which in Fig. 1 are represented by the blue and red curves on the left. Both curves are parameterized by arc length. Then the total energy (4) reduces to

$$E^{\text{pre}} = 2\pi \int_0^{\hat{s}_1} \kappa_H^1 (H - a^1)^2 r_1 ds_1 + 2\pi \int_0^{\hat{s}_2} \kappa_H^2 (H - a^2)^2 r_2 ds_2 + 8\pi\kappa_G - E_a^{\text{pre}}. \tag{12}$$

The adhesion energy between the two axisymmetric separated vesicles should be

$$E_a^{\text{pre}} = 2\pi \int_0^{\hat{s}_1} \left[\int_0^{\hat{s}_2} \int_0^{2\pi} W(\text{dis}) r d\theta ds_2 \right] r ds_1,$$

where θ represents the angle of rotation, and $\text{dis} = |\mathbf{x}_1 - \mathbf{x}_2|$. To simplify our model and the numerical calculation, we drop the effect of the rotation and only consider the adhesive interaction between the two generating curves l_1,l_2, so that a simpler expression reads

$$E_a^{\text{pre}} = 2\pi \int_0^{\hat{s}_1} \left[\int_0^{\hat{s}_2} W(\text{dis}) r ds_2 \right] r ds_1. \tag{13}$$

The constraints (5) become

$$R_1^2(\cos T_1)' = -r_1, \quad R_2^2(\cos T_2)' = -r_2, \tag{14}$$

where R_i are the linear sizes of vesicle Γ_i defined by

$$4\pi R_i^2 = A_i \quad \text{for } i = 1,2, \tag{15}$$

and

$$\pi \int_0^{\hat{s}_1} r_1^2 z_1' ds_1 = V_1, \quad \pi \int_0^{\hat{s}_2} r_2^2 z_2' ds_2 = V_2. \tag{16}$$

One can derive from (12) through (16) the Euler-Lagrange equations, which determine the equilibrium shapes of the two vesicle membranes in the prefusion state, and obtain

$$\begin{aligned} &\widetilde{H}_1'' + \frac{r_1'\widetilde{H}_1'}{r_1} + 2H_1\left(H_1^2 - K_1\right) - 2(\mu_1 H_1 + p_1) - \frac{\delta E_a^{\text{pre}}}{\delta \mathbf{n}_1} = 0, \quad \text{in } \Gamma_1, \\ &\widetilde{H}_2'' + \frac{r_2'\widetilde{H}_2'}{r_2} + 2H_2\left(H_2^2 - K_2\right) - 2(\mu_2 H_2 + p_2) - \frac{\delta E_a^{\text{pre}}}{\delta \mathbf{n}_2} = 0, \quad \text{in } \Gamma_2, \end{aligned} \tag{17}$$

where $\widetilde{H}_i = \kappa_H^i(H_i - a^i)$, $\mathbf{n}_1$ and $\mathbf{n}_2$ are the out normals of Γ_1 and Γ_2, respectively, and the variations $\delta E_a^u/\delta \mathbf{n}_1$ and $\delta E_a^u/\delta \mathbf{n}_2$ are explicitly expressed as

$$\begin{aligned}\frac{\delta E_a^{\rm pre}}{\delta \mathbf{n}_1} &= -\sin\phi_1 \int_0^{\hat{s}_2} \frac{\mathrm{d}(W)}{\mathrm{d}(\mathrm{dis})}\frac{r_1 - r_2}{\mathrm{dis}} r_2 \mathrm{d}s_2 \\ &\quad + \cos\phi_1 \int_0^{\hat{s}_2} \frac{\mathrm{d}(W)}{\mathrm{d}(\mathrm{dis})}\frac{z_1 - z_2}{\mathrm{dis}} r_2 \mathrm{d}s_2 \\ &\quad - 2H_1 \int_0^{\hat{s}_2} W(\mathrm{dis}) r_2 \mathrm{d}s_2, \\ \frac{\delta E_a^{\rm pre}}{\delta \mathbf{n}_2} &= -\sin\phi_2 \int_0^{\hat{s}_1} \frac{\mathrm{d}(W)}{\mathrm{d}(\mathrm{dis})}\frac{r_2 - r_1}{\mathrm{dis}} r_1 \mathrm{d}s_1 \\ &\quad - \cos\phi_2 \int_0^{\hat{s}_1} \frac{\mathrm{d}(W)}{\mathrm{d}(\mathrm{dis})}\frac{z_2 - z_1}{\mathrm{dis}} r_1 \mathrm{d}s_1 \\ &\quad - 2H_2 \int_0^{\hat{s}_1} W(\mathrm{dis}) r_1 \mathrm{d}s_1.\end{aligned} \tag{18}$$

The constants $\mu_i, p_i, i = 1,2$ are the Lagrange multipliers associated with the area and volume constraints (14)–(16).

In the postfusion state, the two axisymmetric vesicles merge into a single axisymmetric vesicle determined by rotating a curve

$$l = [r(s), z(s)], \tag{19}$$

which, in Fig. 1, is the curve on the right and is parameterized by the arc length. Then the total energy (6) reduces to

$$\begin{aligned}E^{\rm post}(\eta) &= 2\pi \int_0^{\hat{s}} \kappa_H(\eta)[H - a(\eta)]^2 r \mathrm{d}s + 4\pi\kappa_G \\ &\quad + 2\pi\sigma \int_0^{\hat{s}} \left[\frac{\xi}{2}\eta'^2 + \Phi(\eta)\right] r \mathrm{d}s - E_a^{\rm post},\end{aligned} \tag{20}$$

with

$$E_a^{\rm post} = \int_0^{\hat{s}} \left[\int_0^{\hat{s}} W(\mathrm{dis}) G(s_1, s_2) r(s_2) \mathrm{d}s_2\right] r(s_1) \mathrm{d}s_1.$$

Notice that the fused vesicle Γ is made up of Γ_1 and Γ_2, so the linear size R of Γ should satisfy

$$R^2 = R_1^2 + R_2^2.$$

And the constraints (10) are replaced by

$$R^2(\cos T)' = -r, \quad \pi \int_0^{\hat{s}} r^2 z' \mathrm{d}s = \mathrm{V}, \tag{21}$$

and

$$2\pi \int_0^{\hat{s}} \eta \mathrm{d}s = 4\pi\left(R_1^2 - R_2^2\right). \tag{22}$$

The equilibrium shapes of the fused vesicle membranes satisfy the Euler-Lagrange equations

$$\begin{aligned}&\widetilde{H}'' + \frac{r'\widetilde{H}'}{r} + 2H(H^2 - K) - 2(\mu H + p + \tau\eta H) \\ &\quad + \sigma\xi\eta'^2\phi' - 2\sigma H\left[\frac{\xi}{2}\eta'^2 + \Phi(\eta)\right] - \frac{\delta E_a^{\rm post}}{\delta \mathbf{n}} = 0, \\ &c_H H^2 + \sigma\left[-\xi\left(\eta'' + \frac{r'\eta'}{r}\right) + \frac{d\Phi}{d\eta}\right] + \tau - \frac{\delta E_a^{\rm post}}{\delta \eta} = 0,\end{aligned} \tag{23}$$

with $\widetilde{H} = \kappa_H(\eta)[H - a(\eta)]$, and the variations of $E_a^{\rm post}$ explicitly expressed as

$$\begin{aligned}\frac{\delta E_a^{\rm post}}{\delta \mathbf{n}} &= -\sin\phi \int_0^{\hat{s}} \frac{\partial W}{\partial[r(s) - r(s_2)]} \widetilde{G}(s, s_2) r(s_2) \mathrm{d}s_2 \\ &\quad + \cos\phi \int_0^{\hat{s}} \frac{\partial W}{\partial[z(s) - z(s_2)]} \widetilde{G}(s, s_2) r(s_2) \mathrm{d}s_2 \\ &\quad - 2H \int_0^{\pi} W \widetilde{G}(s, s_2) r(s_2) \mathrm{d}s_2,\end{aligned} \tag{24}$$

$$\frac{\delta E_a^{\rm post}}{\delta \eta} = \int_0^{\hat{s}} W \frac{\eta(s) - \eta(s_2)}{2} r(s_2) \mathrm{d}s_2, \tag{25}$$

with $\widetilde{G}(s,t) = G(s,t) + G(t,s)$. The constants μ, p, and τ are the Lagrange multipliers associated with constraints (21)–(22).

III. NUMERICAL EXPERIMENTS

To solve the Euler-Lagrange equations, we use the MATLAB solver BVP4C, which is designed for solving the boundary value problems. The interfacial width ξ is taken as $\xi = 0.1, 0.05, 0.02, 0.01$ to test the numerical convergence. As ξ becomes smaller, it is numerically observed that the diffuse interface tends to become sharper, but the vesicle configuration and the geometry of the individual phases remain intact (see [21] for similar testing examples in the case of vesicle-substrate adhesions). Since the convergence of computed results in our numerical simulation has been carefully tested, $\xi = 0.05$ is taken as a representative value for the rest of the paper.

In this section, we present a couple of possible configurations of prefusion and postfusion states, and discuss the diagrams of phase transition for various parameters.

A. Sphere + Sphere → Prolate

One of the most popular *in vitro* experiments of membrane fusion [22,36] is to consider the case where two nearly round vesicles adhere and fuse into a prolate vesicle. This is examined in our first set of numerical experiments. Here we begin with two apposed vesicle membranes in the prefusion state Γ_1, Γ_2, chosen as being almost spherical with their linear sizes, as defined in (15), being set to be equal to $R_1 = 1, R_2 = 1.5$. The volumes are taken as

$$V_1 = \tfrac{4}{3}\pi R_1^3 V_1^{\rm redu}, \quad V_2 = \tfrac{4}{3}\pi R_2^3 V_2^{\rm redu},$$

with the nondimensionalized reduced volumes

$$V_1^{\rm redu} = V_2^{\rm redu} = 0.98.$$

The total area of the fused vesicle is $A_1 + A_2 = 4\pi(R_1^2 + R_2^2)$ and the total volume of the fused vesicle is $V = V_1 + V_2$, so that its reduced volume becomes

$$V^{\rm redu} = \frac{R_1^3 V_1^{\rm redu} + R_2^3 V_2^{\rm redu}}{\left(\sqrt{R_1^2 + R_2^2}\right)^3} = 0.7318.$$

In Fig. 2, we present (on the left) a prefusion equilibrium of two vesicles with an adhesive interaction (adhesion strength $w = 2$). It is obvious that these two vesicles deform due to adhesion, and their shapes become flat in the close-contact

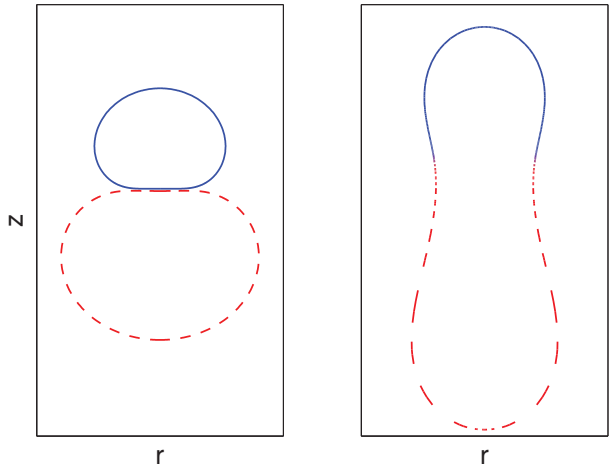

FIG. 2. (Color online) The prefusion and postfusion equilibrium states between two almost round vesicles. The line tension constant σ in the postfusion state is set to be 0.5, and adhesion strength w between blue and red phases equals 2.

region. On the right of Fig. 2, the postfusion equilibrium for the same set of parameters is shown, where a larger prolate vesicle is formed as the two vesicles fuse (the line tension constant is $\sigma = 0.5$). The parameters used are $\kappa_0 = 1$, $c_H = 0$, $a_0 = 0$.

B. Oblate + Oblate → Oblate → Torus

To examine the geometric effects of the adhering vesicle, we next consider two apposed oblate vesicles, instead of two round ones. In this experiment, an interesting fact is revealed by our computation: after two oblate vesicles fuse into a single oblate vesicle, adhesion may further induce the self-fusion into a two-component oblate vesicle, which consequently results in a toroidal shape.

In this case, two apposed vesicle membranes, Γ_1 and Γ_2, in the prefusion state are chosen as being oblate. The linear sizes of the oblates are set to be equal to $R_1 = R_2 = 1$, with smaller reduced volumes $V_1^{\text{redu}} = V_2^{\text{redu}} = 0.75$. Due to the volume conservation of the fusion process, the reduced volume of the fused vesicle is $V^{\text{redu}} = 0.75/\sqrt{2}$.

In Fig. 3, the top diagram presents the equilibrium of apposed two vesicle membranes interacting with each other by adhesion. We point out that this prefusion equilibrium is under an axisymmetric setting. A more general nonsymmetric sigmoid-contact equilibrium [37] might be energetically more favorable than the axisymmetric solution. The middle diagram shows a postfusion equilibrium, where the biconcave membrane is almost in self-contact at the center region. Furthermore, self-fusion could take place and result in an equilibrium state in the shape of a torus, as shown by the bottom diagram of Fig. 3. The other parameter values used are $\kappa_0 = 1$, $c_H = 0$, and $a_0 = 0$.

C. Round + Oblate → Wrapping → Oblate

A recent paper [38] considers the adhesion between a rigid cylindrical particle and a soft fluid membrane tube (both being infinitely long), which causes the wrapping around of the particle by the membrane. This work motivates us to conduct

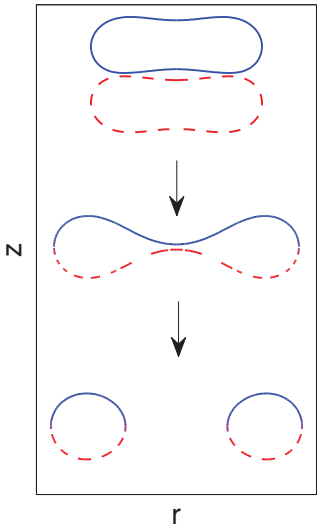

FIG. 3. (Color online) The prefusion and postfusion equilibrium between two oblate vesicle membranes. Adhesion strength $w = 2$, and the line tension $\sigma = 0.5$.

another experiment, in which the fusion between two vesicles is considered, where one is round with a higher bending rigidity (hard) and the other is an oblate with a lower bending rigidity (soft), and the contrast of the bending rigidities is adjusted by the parameter c_H.

For this case, a round vesicle of $R_1 = 1$, $V_1^{\text{redu}} = 0.99$, and an oblate vesicle of $R_2 = 2$, $V_2^{\text{redu}} = 0.6449$, are adhered before the fusion occurs. Consequently a wrapping is formed in the prefusion state. After the fusion process completes, the fused vesicle becomes an oblate with $R = \sqrt{R_1^2 + R_2^2} = \sqrt{5}$ and $V^{\text{redu}} = 0.55$. In Fig. 4, we can see the wrapping effect between two vesicles induced by adhesive interaction. By changing the ratio of bending rigidities of the two vesicles, we observe the wrapping phenomena similar to the findings in [38]. In Fig. 5, we show the prefusion and postfusion equilibrium of the two vesicles, where $\kappa_0 = 1, c_H = 0.5$, namely, the ratio of bending rigidities of the two vesicles $\kappa_H^{\text{blue}}/\kappa_H^{\text{red}} = 3/1$. Due to the combined effects of elastic bending, adhesion, and line tension, the blue phase (with a larger bending modulus) of the postfusion equilibrium in Fig. 5 is nearly flat, while the red phase (with a smaller bending modulus) curves dramatically.

D. Phase transitions

To further study the vesicle fusion induced by adhesion, one interesting numerical experiment is to detect the role that

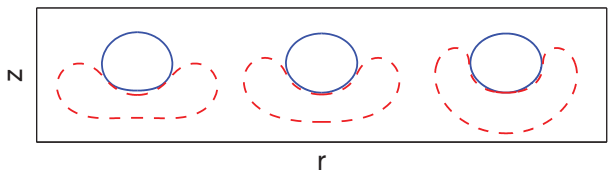

FIG. 4. (Color online) The wrapping induced by adhesive interaction between a soft oblate and a hard, almost round vesicle. $\kappa_0 = 1; c_H = 0.05, 0.5, 0.8$, from left to right, respectively.

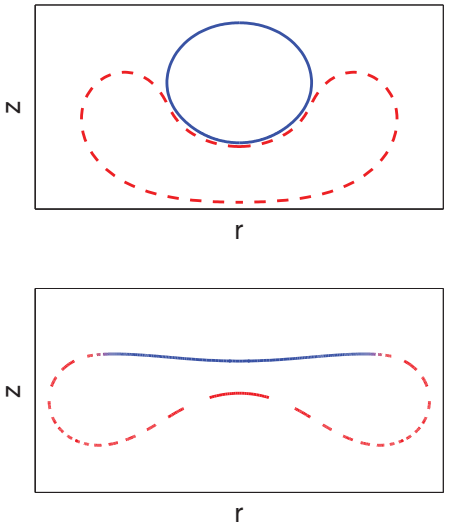

FIG. 5. (Color online) The prefusion and postfusion equilibrium states of the wrapping case for $w = 2$. The line tension constant $\sigma = 0.5$ in the postfusion state, and $\kappa_0 = 1, a_H = 0.5$ yields $\kappa_H^{\text{blue}}/\kappa_H^{\text{red}} = 3/1$.

adhesion strength w plays in the process of vesicle fusion. Here we consider the fusion between two almost round vesicles, as we did in Sec. III A. All the other parameters are kept fixed. A simple relation determines the $w - \kappa_G$ transition,

$$\left(E_{\text{b}}^{\text{post}} + E_{\text{l}}^{\text{post}} - E_{\text{a}}^{\text{post}}\right) - \left(E_{\text{b}}^{\text{pre}} - E_{\text{a}}^{\text{pre}}\right) = 4\pi\kappa_{\text{G}}. \quad (26)$$

In Fig. 6, the $w - \kappa_G$ diagram of the phase transition from prefusion to postfusion is presented on the left. In a similar manner, the $c_H - \kappa_G$ diagram of the phase transition from prefusion to postfusion is shown on the right. Above both transition curves, the postfusion state is energetically more favorable than the prefusion state; while below each curve, the prefusion equilibrium becomes more favorable energetically.

We can further simulate the exocytosis equilibrium, fusion, and endocytosis equilibrium between a plasma membrane and a vesicle with adhesive interaction. In this experiment, we take the linear size of the vesicle $R_1 = 1$, and the linear size of the plasma membrane $R_2 = 4$, with reduced volumes $V_1^{\text{redu}} = 0.98$, $V_2^{\text{redu}} = 0.9347$. Then the linear size of the fused membrane $R = \sqrt{17}$, and its reduced volume is computed as $V^{\text{redu}} = 0.8674$. Figure 7 presents equilibrium shapes in exocytosis, fusion, and endocytosis with parameters given as above. The spontaneous curvatures on two separated

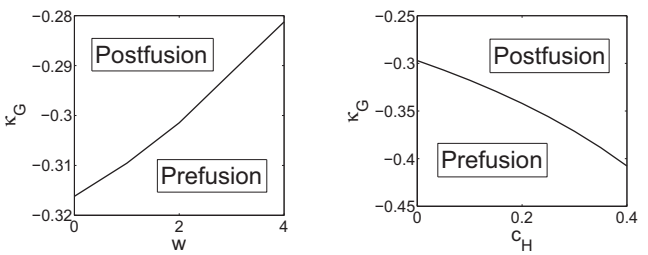

FIG. 6. Left: $w - \kappa_G$ diagram of phase transition from prefusion to postfusion. Right: $c_H - \kappa_G$ diagram of phase transition from prefusion to postfusion.

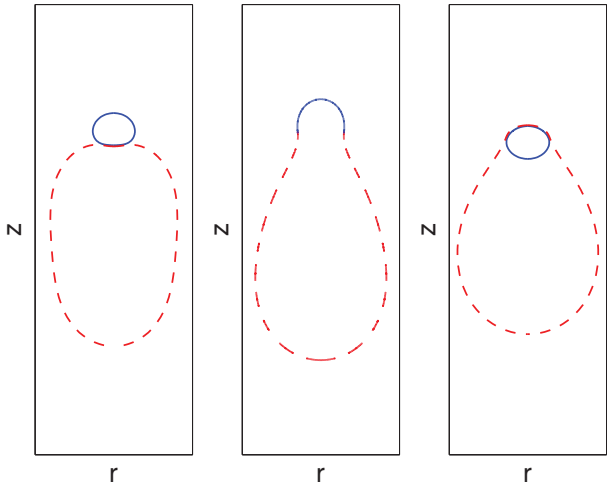

FIG. 7. (Color online) Left to right: Exocytosis, fusion, and endocytosis equilibria. The spontaneous curvatures on two separated membranes are $a^1 = 0.5, a^2 = 0$, with $a_0 = 0.25, a_H = 1$ in the fusion equilibria.

membranes are distinct with $a^1 = 0.5$ and $a^2 = 0$. To compare which one of the three equilibrium states is energetically more favorable, the diagram of E^{total} versus a_0 is shown in Fig. 8, where $\kappa_G = 0$ is assumed. Two energy transition points, $a_{\text{L}} = 0.2328$ and $a_{\text{R}} = 0.6602$, are found. When $a_0 < a_{\text{L}}$, the fusion equilibrium has the lowest energy among the three states; as $a_{\text{L}} < a_0 < a_{\text{R}}$, the energy of the exocytosis is larger than that of the fusion state and both of them are larger than the energy of endocytosis, i.e., in this region of a_0, without having to overcome any energy barrier, the vesicle that was originally outside of the plasma membrane can be successfully fused with the plasma membrane, and finally step into the plasma membrane by endocytosis. Finally, if $a_0 > a_{\text{R}}$, the energetic order changes and the energy decreases as the vesicles change from fusion to exocytosis and then to endocytosis. The influence of Gaussian modulus κ_G on the transition points a_{L} and a_{R} is presented in Fig. 9. The three

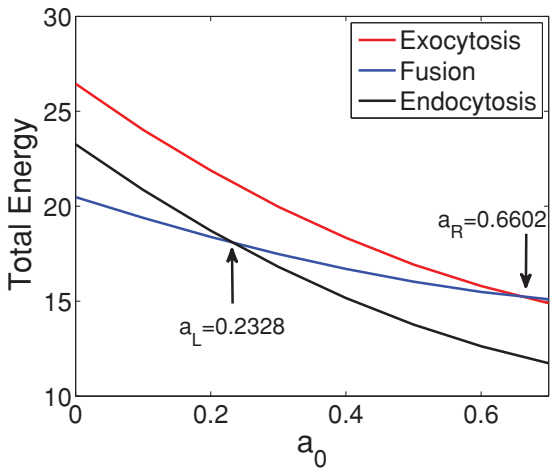

FIG. 8. (Color online) Energy comparison between exocytosis, fusion, and endocytosis equilibria, where a_{L} and a_{R} are the two transition points.

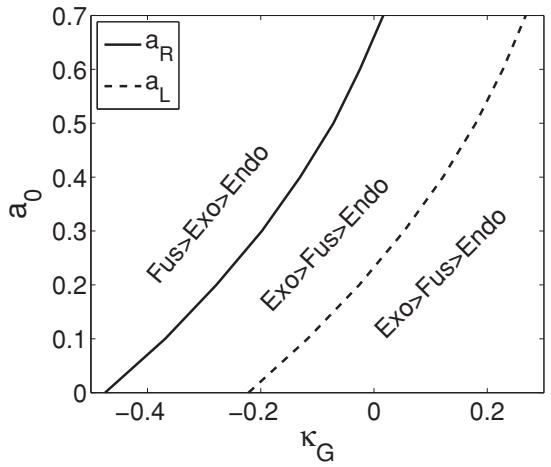

FIG. 9. The phase transition diagram of κ_G vs a_0. The solid and dashed curves represent the dependence of the transition points a_L and a_R on the Gaussian bending modulus. The three states, exocytosis, fusion and endocytosis, are ordered by the total energy in different regions.

regions determined by $\kappa_G - a_L$ and $\kappa_G - a_R$ are shown. For each of the regions, the three equilibrium states are ordered by their total energies.

E. Dynamic simulations

In addition to the study of equilibria, it is highly desirable to generalize our analysis and simulations to cover the dynamic fusion process. In reality, the model studied in the present work cannot fully account for the whole fusion process, especially the hemifusion state, which is affected by many other important factors. The latter has remained a very active area of research. In the present context, it is illuminative to conduct the dynamic simulations based on the model given here to illustrate the transitions to the prefusion and postfusion states. This allows us to estimate the various energetic contributions to the vesicle fusion process.

To be specific, we consider the following dynamic system:

$$\frac{d\Gamma}{dt} = -\frac{\delta E}{\delta \Gamma}, \tag{27}$$

where t is the time variable, Γ is the vesicle surface in the prefusion or postfusion state, and $E = E^{\text{pre}}$ or E^{post} is the total energy of the system.

Figure 10 ($A \to D$) schematically presents the gradient flow dynamics of the fusion process. In this figure, two vesicles are placed in the prefusion equilibrium. We postulate that due to adhesion and thermal fluctuations, there are two main steps in the fusion process: namely, the energy barrier crossing and the transition to the postfusion equilibrium. In the first step ($A \to B$), two vesicles in prefusion equilibrium are pulled together, due to adhesion and fluctuation forces, to make contact at a single point. Since the energy of the vesicles in such a position is higher than the prefusion and postfusion equilibria, we describe this step through a time-reversal process, that is, we solve for the gradient dynamics from the state B to A. After reparameterizing the two vesicles in contact and representing them as the surface of a single vesicle, we

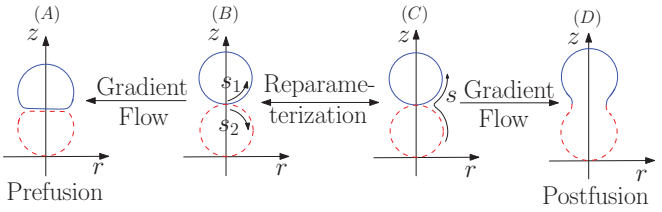

FIG. 10. (Color online) Schematic of fusion process ($A \to D$) by gradient flow dynamics. The figures ($B \to A$) present the gradient flow dynamics from two single-point-contact vesicles to a prefusion state. The reverse process ($A \to B$) describes the process where extra work is done to push the prefused vesicles to make contact. The two vesicles in (B) are viewed as a single vesicle in (C) after reparameterization, and the gradient flow dynamics ($C \to D$) present the pore formation and the final postfusion equilibrium.

then conduct the gradient flow dynamics ($C \to D$) to reach the postfusion equilibrium. The two steps of such a gradient flow dynamics can be justified from the large deviation theory about rare events of energy barrier crossing.

For illustrative purposes, two identical axisymmetric vesicles, Γ_1 and Γ_2, with $R_1 = R_2 = 1/\sqrt{2}$, $V_1^{\text{redu}} = V_2^{\text{redu}} = 0.99$, are set initially to be in contact with each other. Due to the adhesion effect ($w = 2$), the gradient flow dynamics (27) leads the vesicles to the prefusion equilibria. We may use the reverse process of this gradient flow dynamics to mimic the first step of the fusion process. For the second step, the two contacting vesicles are reparameterized using a single parameter in order to represent the instantaneous state prior to the pore formation. Figure 11 presents numerical simulations of the gradient dynamics. The number under each profile is the corresponding total energy. The top figure (a) presents the first step of the gradient flow, where two vesicles in prefusion equilibria ($A1$) are making contact with each other

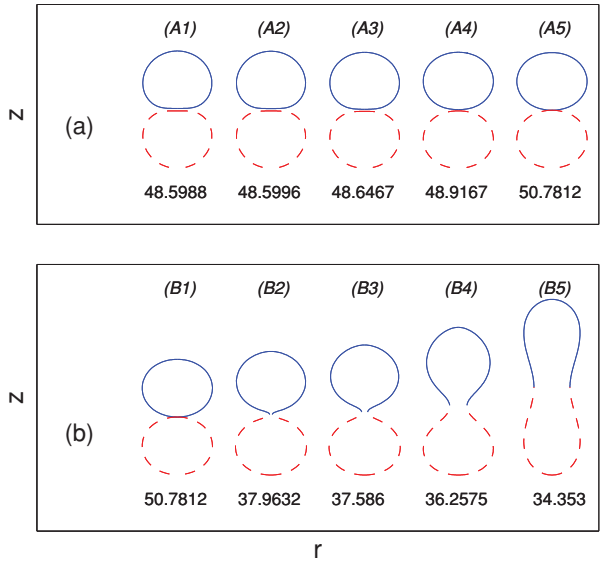

FIG. 11. (Color online) Fusion process by gradient flow dynamics. The energy barrier is in the single-point-contact state ($A5$) and its reparameterization ($B1$), which corresponds to the hemifusion state. The values of the parameters are $\kappa_H = \kappa_G = 1$, $R_1 = R_2 = 1/\sqrt{2}$, $V_1^{\text{redu}} = V_2^{\text{redu}} = 0.99$, $w = 2$, $\sigma = 2$.

(*A*5). After reparameterizing the profile (*A*5), we reformulate the vesicles in contact as a single vesicle, which is given again in (*B*1). By following the gradient flow dynamics with the reparameterized profile, one can observe the pore formation in (*B*2), with the pore size continuing to increase until the postfusion equilibrium (*B*5) is reached. We note that the dramatic drop in the total energy from (*B*1) to (*B*2) is mostly due to the sharp drop of the Gaussian energy contribution.

Since the simple sharp interface approach adopted in this study lacks a detailed description of the hemifusion state, the energy computed here for the initial in-contact state serves only as an estimation of the upper bound of the actual energy barrier. It will be of great interest to conduct more detailed studies of the hemifusion state and the energy barrier; some alternatives employing an implicit surface representation are discussed in Sec. IV.

IV. CONCLUSION

In the current work, we have introduced and studied a continuum diffuse interface model for the lipid membrane fusion process, which incorporates the nonlocal adhesion effect and other energetic contributions. A phase transition diagram with respect to adhesion strength, bending, and Gaussian moduli, and the spontaneous curvature, can be built up systematically through numerical computations. In many *in vitro* experiments of the membrane fusion [22,36], it has been very popular to examine the case where two round vesicles merge into a prolate one. Our study reveals that there can be many other interesting equilibrium configurations of the prefusion and postfusion states, suggesting further theoretical and experimental investigations.

Our model can be extended in a number of directions. By adding one more phase field function to describe membranes themselves [34], we may further examine the fusion intermediate or the hemifusion state, which could lead to more accurate information regarding the energy barriers between the prefusion and postfusion states. We may also introduce inhomogeneities into the energy functionals to model the effect of transmembrane proteins on the fusion process more closely. Such works can allow a more quantitative comparison with the popular stalks model. Additionally, while we have made preliminary studies of the gradient dynamics, there are a large variety of other fusion dynamic processes which can also be examined.

ACKNOWLEDGMENTS

The research is supported in part by NSF Grant No. DMS-1016073 and NIH Grant No. NCI-CA125707. The authors thank the referees for many interesting suggestions, including those on the study of the dynamic fusion processes.

[1] R. Blumenthal, M. J. Claugue, S. R. Durell, and R. M. Epand, Chem. Rev. **103**, 53 (2003).
[2] L. V. Chernomordik and M. M. Kozlov, Nature Struct. Mol. Biol. **15**, 675 (2008).
[3] P. L. Yeagle, *The Membrane of Cells* (Academic, New York, 1993).
[4] D. M. Knipe and P. M. Howley, *Fields Virology* (Lippincot Williams & Wilkins, New York, 2007).
[5] A. Chanturiya, L. V. Chernomordik, and J. Zimmerberg, Proc. Natl. Acad. Sci. USA **94**, 14423 (1997).
[6] L. V. Chernomordik, G. B. Melikyan, and Y. A. Chizmadzhev, Biochim. Biophys. Acta. **906**, 309 (1987).
[7] F. S. Cohen, J. Zimmerberg, and A. Finkelstein, J. Gen. Physiol. **75**, 251 (1980).
[8] V. S. Malinin, P. Frederik, and B. R. Lentz, Biophys. J. **82**, 2090 (2002).
[9] L. Yang and H. W. Huang, Biophys. J. **84**, 1808 (2003).
[10] M. M. Kozlov and V. S. Markin, Biofizika. **28**, 242 (1983).
[11] Y. Kozlovsky, L. Chernomordik, and M. M. Kozlov, Biophys. J. **83**, 2634 (2002).
[12] Y. Kozlovsky, A. Efrat, D. P. Siegel, and M. M. Kozlov, Biophys. J. **87**, 2508 (2004).
[13] Y. Kozlovsky and M. M. Kozlov, Biophys. J. **82**, 882 (2002).
[14] V. Markin and J. Albanesi, Biophys. J. **82**, 693 (2002).
[15] M. Muller, K. Katsov, and M. Schick, Biophys. J. **85**, 1611 (2003).
[16] H. Noguchi and M. Takasu, Phys. Rev. E **64**, 041913 (2001).
[17] H. Noguchi and M. Takasu, J. Chem. Phys. **115**, 9547 (2001).
[18] A. Grafmuller, J. Shillcock, and R. Lipowsky, Phys. Rev. Lett. **98**, 218101 (2007).
[19] J. C. Shillcock and P. Lipowsky, Nature Mater. **4**, 225 (2005).
[20] R. Lipowsky and U. Seifert, Mol. Cryst. Liq. Cryst. **202**, 17 (1991).
[21] Y. Zhao, S. Das, and Q. Du, Phys. Rev. E **81**, 041919 (2010).
[22] R. Lipowsky, Nature (London) **349**, 475 (1991).
[23] W. Helfrich, Z. Naturforsch. C **28**, 693 (1973).
[24] C. M. Chen, P. G. Higgs, and F. C. MacKintosh, Phys. Rev. Lett. **79**, 1579 (1997).
[25] C. Elliott and B. Stinner (unpublished).
[26] C. M. Funkhouser, F. J. Solis, and K. Thornton, Phys. Rev. E **76**, 011912 (2007).
[27] Y. Jiang, T. Lookman, and A. Saxena, Phys. Rev. E **61**, R57 (2000).
[28] T. Kawakatsu, D. Andelman, K. Kawasaki, and T. Taniguchi, J. Phys. II (France) **3**, 971 (1993).
[29] J. Lowengrub, A. Ratz, and A. Voigt, Phys. Rev. E **79**, 031926 (2009).
[30] J. L. McWhirter, G. Ayton, and G. A. Voth, Biophys. J. **87**, 3242 (2004).
[31] Y. Oya, K. Sato, and T. Kawakatsu, e-print arXiv:1011.3868.
[32] T. Taniguchi, Phys. Rev. Lett. **23**, 4444 (1996).
[33] J. S. Sohn, Y. H. Tseng, S. W. Li, A. Voigt, and J. Lowengrub, J. Comput. Phys. **229**, 119 (2010).
[34] X. Wang and Q. Du, J. Math. Biol. **56**, 347 (2008).
[35] Q. Du, Philos. Mag. **91**, 165 (2011).
[36] C. K. Haluska, K. A. Riske, V. Marchi-Artzner, J. Lehn, and R. Lipowsky, Proc. Natl. Acad. Sci. USA **103**, 15841 (2006).
[37] P. Ziherl and S. Svetina, Proc. Natl. Acad. Sci. USA **104**, 761 (2006).
[38] J. Z. Y. Chen and S. Mkrtchyan, Phys. Rev. E **81**, 041906 (2010).